

## Real-Time View of Mesoscopic Surface Diffusion

K. R. Roos,<sup>1,2,\*</sup> K. L. Roos,<sup>1</sup> I. Lohmar,<sup>3</sup> D. Wall,<sup>1</sup> J. Krug,<sup>3</sup> M. Horn-von Hoegen,<sup>1</sup> and F.-J. Meyer zu Heringdorf<sup>1,†</sup>

<sup>1</sup>*Department of Physics and Center for Nanointegration Duisburg-Essen (CeNIDE), Universität Duisburg-Essen, D-47057 Duisburg, Germany*

<sup>2</sup>*Department of Physics, Bradley University, Peoria, Illinois 61625, USA*

<sup>3</sup>*Institut für Theoretische Physik, Universität zu Köln, 50937 Köln, Germany*

(Received 10 August 2007; published 8 January 2008)

Photoemission electron microscopy is used to study the thermal decay of Ag islands grown epitaxially on Si(001) surfaces. ( $2 \times 3$ ) Ag reconstructed zones, due to migrating Ag atoms supplied to the surface by the decaying islands, surround each of the islands. The shape of these reconstructed zones depends on the degree of diffusion isotropy in the system. We demonstrate that the imaging of these reconstructed “isocoverage zones” constitutes a unique experimental method for directly observing diffusion fields in epitaxial systems. We describe the dynamics of the thermal decay of the islands and the isozones in the context of a continuum diffusion model.

DOI: [10.1103/PhysRevLett.100.016103](https://doi.org/10.1103/PhysRevLett.100.016103)

PACS numbers: 68.35.Fx, 68.37.Nq, 68.43.Vx

Surface diffusion is an important physical process that mediates thin film growth and the formation of nanostructures at surfaces. In many instances, however, it is impossible to directly observe diffusive mass transport, and knowledge of the mediating diffusion must be inferred from morphological aspects and/or spatial correlations of the structures formed. One example, wherein diffusion parameters are obtained by inspecting the mediated structures, is the well-known island counting method in scanning tunneling microscopy (STM) [1]. Direct visualization of specific diffusion events, on the other hand, is possible by watching single atoms hop on small terraces in field ion microscopy (FIM) [2], by following atoms on the surface in atom-tracer STM [3], or by video STM [4,5]. The application of these methods, however, will always be restricted to a few atoms in small fields of view at relatively low temperatures. But, it is frequently the collective effects of all the individual surface diffusion processes at the mesoscopic scale, and the degree of the resulting isotropy inherent in diffusive systems, that are invoked to explain ordering at surfaces and the formation of nanostructures [6–10]. This mesoscopic-scale diffusion, that is, the rapid, chaotic mobility of hundreds of thousands of atoms, remains difficult to directly behold. In spite of this difficulty, with the advent of element-selective microscopy, large scale diffusion fields have been studied. Typically, this has been accomplished by observing the diffusion-mediated shape-changes, or the filling-in with diffusing entities, of artificially created structures [11–13]. For instance, a patch of material that is deposited through a shadow mask spreads out during annealing. Modeling of the spreading provides access to fundamental diffusion parameters. Such quench-and-look experiments, however, describe a complicated 3D situation far from equilibrium as the patch would ultimately attempt to cover the whole surface if given enough time.

In this Letter we describe a method for producing reliable representations of a surface diffusion field, the dy-

namics of which we are able to observe in real time at high temperatures with great ease using photoemission electron microscopy (PEEM).

The experiments were performed in an ultrahigh vacuum (UHV) low energy electron microscope (LEEM) [14]. Well oriented Si(001) and vicinal (miscut by  $4^\circ$  in the [110] direction) Si(001) substrates, were cleaned by standard flash-annealing after degassing at  $600^\circ\text{C}$  in UHV for several hours. Ag was evaporated thermally from a ceramic crucible, and the growth of the Ag deposits at elevated substrate temperatures ( $500\text{--}600^\circ\text{C}$ ) was monitored *in situ* with PEEM or LEEM. At these deposition temperatures the initial Ag deposit forms a ( $3 \times 2$ ) Ag reconstruction [15], and subsequent deposition produces compact epitaxial islands and nanowires on top of this reconstructed layer [9]. The islands exhibit various shapes and sizes [16], they are single-crystalline, and have defined side facets. After deposition, the Ag island decay experiments were performed at  $\approx 650^\circ\text{C}$ .

Figure 1 shows PEEM images taken during desorption of Ag on flat Si(001) at  $650^\circ\text{C}$ . The isolated Ag island is the small bright feature near the center in each panel. During annealing the surface breaks up into bright and dark regions. The large bright zone around each island, once formed, decays rapidly into a smaller steady-state size that, thereafter, decreases much more slowly. The island decays simultaneously, and the bright zone eventually disappears only when the island has completely vanished. Figure 1(e) shows the bright zone about to disappear right after the compact island is completely gone, and Fig. 1(f) shows the surface after the disappearance of the bright zone.

Figure 2 shows the time dependence of the island radius and the bright zone radius of Fig. 1 during the decay. Three decay regimes for the bright zone are readily observed: (i) the initial rapid relaxation, (ii) the nearly constant “steady-state” regime, and (iii) the rapid decay of the bright zone once the island has completely disappeared. This decay behavior is typical of all the islands studied at

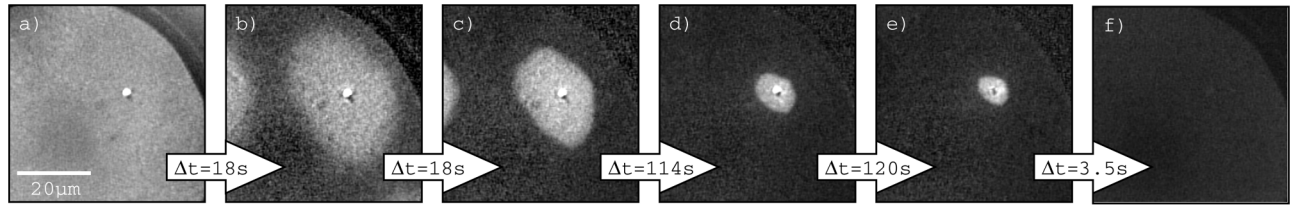


FIG. 1. A series of PEEM images illustrating the thermal decay of a Ag island on flat Si(001), and the formation and decay of the bright zone around the island. The curved line in the upper right corner of each image is the edge of the channel plate used for image intensifying. The substrate temperature ( $\approx 650^\circ\text{C}$ ) and the length scale is the same in all the images. See [23] for a PEEM movie of the thermal decay of a Ag island on Si(001), produced *in situ* and in real time.

this desorption temperature. It is important to note that the bright zones can be observed only over a very narrow temperature range. At temperatures below  $640^\circ\text{C}$  there is very little desorption, and no bright zones are produced. With increasing temperature, the duration of region II in Fig. 2 decreases. Around  $690^\circ\text{C}$  desorption is so rapid that a steady state can no longer be observed, and the zone radius decreases monotonically to zero. For temperatures much higher than  $690^\circ\text{C}$  massive desorption inhibits the zones' formation.

That a bright zone forms around the island and disappears only after the island has vanished suggests that the island, as it decays, feeds atoms onto the surface, and that the bright zone surrounding the decaying island is due to a net adatom diffusion current directed away from the island. We have used microdiffraction to analyze the contrast mechanism behind the different features in the PEEM images. The microdiffraction patterns from the dark regions reveal the typical diffraction pattern of a well-ordered,  $(2 \times 1)$  reconstructed Si(001) surface, although a dilute lattice gas of Ag adatoms is most likely also present. Microdiffraction from the bright zones surrounding the Ag islands reveals a  $(3 \times 2)$  Ag diffraction pattern. Thus, the contrast in the PEEM images of the decaying Ag islands arises from the difference in electronic structure between  $(2 \times 1)$  Si and  $(3 \times 2)$  Ag, with the bright areas around the islands corresponding to the  $(3 \times 2)$  Ag reconstructed overlayer.

Since a critical coverage of Ag ( $\theta^* = 2/3 \text{ ML}$  [17]) is needed for the  $(3 \times 2)$  Ag to form, the boundary between the bright  $(3 \times 2)$  Ag reconstructed areas and the dark  $(2 \times 1)$  reconstructed Si areas is where the Ag coverage exactly equals the critical coverage  $\theta^*$ . This isocoverage line encompasses the bright zones which, for the remainder, we will refer to as “isocoverage-zones” (ICZs). The Ag coverage inside the ICZ boundary is sufficiently high ( $>\theta^*$ ) to form the  $(3 \times 2)$  Ag reconstruction, and outside the ICZ the coverage is too low ( $<\theta^*$ ) to yield the Ag reconstruction. Since the ICZ boundary defines the extent of the  $(3 \times 2)$  Ag formation, and the  $(3 \times 2)$  Ag formation in turn is determined by the diffusion of Ag atoms from the source, the ICZ's shape constitutes a reliable “footprint” of the effective diffusion field.

In order to understand the underlying mechanism for the formation of the ICZ in more detail and to link our obser-

vation to the actual diffusion parameters we formulate a simple diffusion model for the steady-state condition. The central quantity of interest is the local Ag coverage  $\theta(\vec{r})$ . We assume that for  $\theta < \theta^*$  the Ag atoms form a dilute lattice gas with diffusion coefficient  $D$  and desorption rate  $1/\tau$ . The experiments indicate that once the local coverage exceeds  $\theta^*$ , a  $(3 \times 2)$  Ag reconstruction is formed. Accordingly, we assume that only the excess coverage  $\phi(\vec{r}) = \theta(\vec{r}) - \theta^*$  is mobile and can desorb, with modified diffusion coefficient  $\tilde{D}$  and desorption rate  $1/\tilde{\tau}$ . The sudden onset of Ag mobility when the coverage falls below  $\theta^*$  may seem like a drastic oversimplification, but the results that follow do not crucially depend on it. In the quasistatic approximation for a circular geometry the coverage satisfies

$$D\nabla^2\theta(r) - \theta(r)/\tau = 0, \quad \theta(r) < \theta^*, \quad (1)$$

and a similar equation holds for  $\phi(r)$  with coefficients  $\tilde{D}$  and  $\tilde{\tau}$ . At the ICZ perimeter the boundary conditions  $\theta = \theta^*$  and  $\phi = 0$  must be fulfilled. The diffusion and desorption parameters define the diffusion lengths  $x_s = \sqrt{D\tau}$  and  $\tilde{x}_s = \sqrt{\tilde{D}\tilde{\tau}}$  in the unreconstructed and reconstructed regions, respectively. Denoting the corresponding activation energies for diffusion and desorption by  $E_D, E_\tau$  and  $E_{\tilde{D}}, E_{\tilde{\tau}}$  and assuming a common attempt frequency for all processes, we have

$$x_s = a \exp[(E_\tau - E_D)/2k_B T] \quad (2)$$

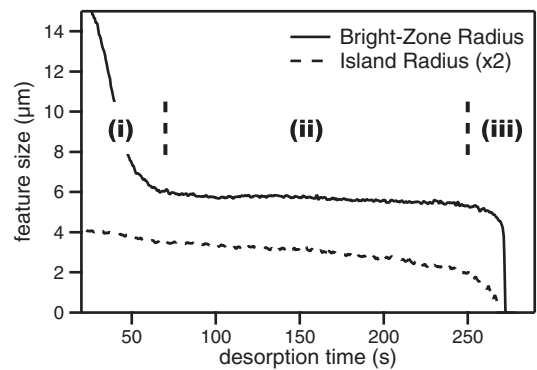


FIG. 2. The time dependence of the radii of the Ag island and the surrounding bright zone shown in Fig. 1. The radii are measured from the center of the island. Three different regimes are indicated: (i) formation of the bright zone, (ii) steady-state regime, (iii) decay regime.

and

$$\tilde{x}_s = a \exp[(E_{\bar{\tau}} - E_{\bar{D}})/2k_B T], \quad (3)$$

where  $a \approx 7 \text{ \AA}$  is the mean square jump length of a single atom jump for diffusion parallel and perpendicular to the dimer rows [18].

We consider a circular diffusion zone of radius  $R$  enclosing a circular Ag island of radius  $R_0 < R$ . The general solution of the stationary diffusion Eq. (1) can be expressed in terms of modified Bessel functions. The boundary condition at the island edge is  $\phi(R_0) = \phi_0$ , where  $\phi_0$  is the excess Ag coverage supplied by the dissolving island. The stationary zone radius  $R$  is determined by the continuity of the current of diffusing Ag atoms across the zone boundary, where  $\phi(R) = 0$  and  $\theta(R) = \theta^*$ . It can be shown that such a stationary solution always exists, and that it is dynamically stable. Moreover, parameter studies of the solution suggest that the selected zone radius can be considerably larger than the island radius,  $R \gg R_0$  (as is experimentally observed), only if  $R$  is small compared to both diffusion lengths,  $R \ll x_s, \tilde{x}_s$ . This will therefore be taken to be the case in the following. The relation between zone radius and island radius then reduces to a simple power law,

$$R = x_s (R_0/x_s)^\nu, \quad (4)$$

where  $\nu = [1 + (\tilde{D}/D)(\phi_0/\theta^*)]^{-1} < 1$ .

All islands that we analyzed experimentally follow the typical time-dependent behavior shown in Fig. 2 and in the stationary regime show a power law behavior as expected from Eq. (4). One example for the  $R$  vs  $R_0$  dependence is plotted in Fig. 3 in a double-logarithmic plot. A fit with Eq. (4) allows the determination of  $x_s$  and  $\nu$ . Most of the islands analyzed give a range of values for  $\nu$  between 0.2 and 0.8, and reasonable values of  $x_s$ . Selected, well separated islands that exhibit a symmetrical ICZ and that display a typical decay behavior like that shown in Fig. 2, yield values for  $\nu$  between 0.5 and 0.7, and values for  $x_s$  around  $500 \mu\text{m}$ .

Comparing these results to Eq. (2) we arrive at  $E_{\bar{\tau}} - E_{\bar{D}} \approx 2.3 \text{ eV}$ . This is consistent with a density functional

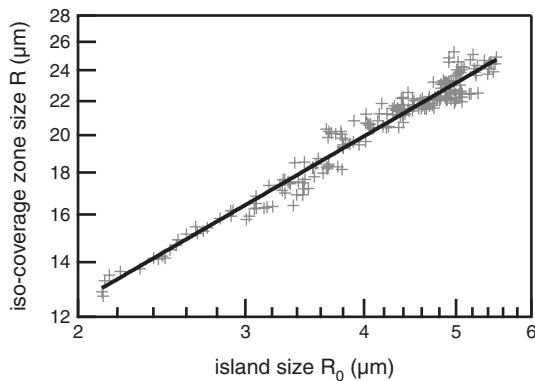


FIG. 3. The ICZ radius vs island radius in the steady-state regime for a decaying Ag island on flat Si(001).

(DFT) study of diffusion of Ag on unreconstructed Si(001) [18], which finds  $E_{\bar{\tau}} = 3.1 \text{ eV}$  and  $E_{\bar{D}} = 0.5 \text{ eV}$  for both Ag monomers and dimers migrating parallel to the dimer rows, hence  $E_{\bar{\tau}} - E_{\bar{D}} = 2.6 \text{ eV}$ . The exponent we measure,  $\nu \approx 0.6$ , implies that  $\tilde{D}/D \approx (2/3)(\theta^*/\phi_0) = 4/(9\phi_0)$ . A plausible value for the excess coverage at the island boundary is  $\phi_0 \approx 1$ , which translates into a difference of  $E_{\bar{D}} - E_D \approx 0.1 \text{ eV}$  between the diffusion barriers in the reconstructed and unreconstructed regions. Together with the DFT estimate  $E_D = 0.5 \text{ eV}$  this yields  $E_{\bar{D}} \approx 0.6 \text{ eV}$ , which is somewhat smaller than, but not inconsistent with the estimate  $E_{\bar{D}} = 0.7 \text{ eV}$  obtained from a nucleation study [19].

Finally, we need to verify the consistency of our assumption that  $\tilde{x}_s \gg R$ . Requiring that  $\tilde{x}_s > 100 \mu\text{m}$ , say, implies that  $E_{\bar{\tau}} - E_{\bar{D}} > 2 \text{ eV}$ , or  $E_{\bar{\tau}} > 2.6 \text{ eV}$ . This is consistent with the lower bound of  $2.1 \text{ eV}$  on the desorption barrier obtained in Ref. [19]. We conclude, therefore, that the interpretation of the ICZ formation within the simple diffusion theory yields estimates of several microscopic parameters which are in good agreement with previously available information on the Ag/Si(001) system. While the actual diffusion length  $x_s$  is much larger than the radius of the ICZ, a consequence of the relation (4), the good agreement of the diffusion parameters from the model with values from the literature indicates, that in fact the ICZs do reliably represent a footprint of the effective diffusion field of the island.

This method of “diffusion-contrast” imaging in PEEM provides a mesoscopic view of diffusion in a system without the cumbersome task of needing to know the details of all the active surface diffusion processes. Such experimental information has important ramifications for the relative ease with which knowledge of the effective diffusion in a particular system can be obtained. For example, it may not be surprising that, for a flat Si(001) surface, with a sequence of terraces whose dimer rows are rotated by  $90^\circ$  from terrace to adjacent terrace, the effective two-dimensional diffusion field is isotropic since any anisotropy-inducing atomistic processes would be averaged out over the many terraces within the ICZ. This situation is depicted in the PEEM image of Fig. 4(a), where several Ag islands and their associated ICZs are seen decaying on a flat Si(001) surface. But when a net anisotropy is introduced into a system, as in the case of Ag islands decaying on single-domain [20] vicinal Si(001), it is not obvious, without an intimate knowledge of the surface diffusion barriers, what the predominant diffusion channel will be. Shown in Fig. 4(b) is a PEEM image of Ag islands and the accompanying ICZs decaying on vicinal Si(001). The dashed line in Fig. 4(b) indicates the direction of the steps of the vicinal surface. In contrast to the circular symmetry on flat Si(001), the vicinal ICZs display a highly eccentric elliptical shape, reflecting a high degree of anisotropy in the surface diffusion.

We believe that the imaging of ICZs is a useful addition to the toolset of diffusion analysis and provides insight into

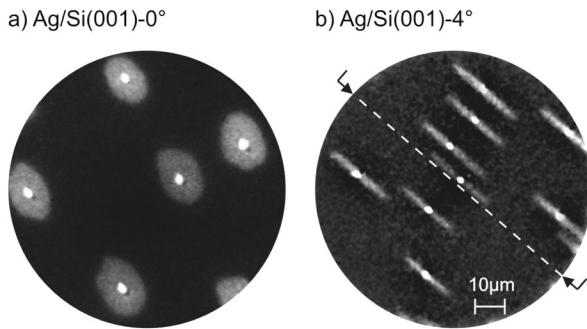


FIG. 4. Decaying Ag islands and ICZs in the steady-state regime on (a) flat and (b) vicinal Si(001) at 650 °C. The substrate steps on the vicinal surface are parallel to the dashed line in (b). The scale is the same in both images.

the collective effects of surface diffusion processes in specific epitaxial systems beyond the well-established methods of observing island decay and/or island separation. Such techniques focus on the presence, shape, and distribution of islands rather than on a fast reacting adatom concentration in a reconstruction. Island shape can be misleading if determining diffusive anisotropy in a system is desired. For example, we have experimentally observed that the compact shape of the grown and decaying Ag islands are the same on Si(001) surfaces, independent of the vicinity. Furthermore, the island density, and therefore the average island separation, is virtually the same for the two dramatically different surfaces we used in this study. The island density, alone, would thus not provide any clue to the anisotropic nature of the vicinal surface. In fact, it is well known that only in cases of extreme anisotropic diffusion [21,22] a small, subtle effect on nucleation can be observed, and elaborate analysis is needed to extract the anisotropy. In contrast, the aspect ratio of the vicinal ICZ of roughly ten is strikingly high, compared to that for the flat surface (approximately one). This ICZ aspect ratio measurement is sufficient to conclude that there is a significant amount of diffusion anisotropy in the system. In this way, the imaging of the ICZ as a representation of the diffusion field greatly extends the possibilities for gaining further understanding of diffusion and diffusion anisotropy at surfaces.

We note, finally, that we have observed Ag ICZs on a variety of other vicinal and patterned Si surfaces, and that the ICZ imaging method appears to be a broadly applicable method for visualizing diffusion. In the case of the ICZs we observe, the electronic structure of the overlayer is clearly different from that of the Ag islands and the Si substrate. Since any overlayer will have an electronic structure different from that of the substrate and the decaying island that is feeding the overlayer, we conclude that many metal adatom-induced overlayers surrounding the decaying islands on a surface should produce a similar distinguishable contrast in PEEM, and that the procedure described herein can be used to image diffusion fields in a wide array of heteroepitaxial systems.

Financial support from the Deutsche Forschungsgemeinschaft through No. SFB616 “Energy Dissipation at Surfaces” and SFB-TR 12 “Symmetries and universality in mesoscopic systems” is gratefully acknowledged. Kelly Roos acknowledges financial support from the National Science Foundation (No. DMR-0511811), and from the Cottrell College Science Grant program of the Research Corporation. We are grateful to Thomas Michely and Peter Kury for fruitful discussions.

\*rooster@bradley.edu

†meyerzh@uni-due.de

- [1] H. Brune, G. S. Bales, J. Jacobsen, C. Boragno, and K. Kern, *Phys. Rev. B* **60**, 5991 (1999).
- [2] G. Ehrlich and F.G. Hudda, *J. Chem. Phys.* **44**, 1039 (1966).
- [3] B. S. Swartzentruber, *Phys. Rev. Lett.* **76**, 459 (1996).
- [4] F. Besenbacher, F. Jensen, E. Lægsgaard, K. Mortensen, and I. Stensgaard, *J. Vac. Sci. Technol. B* **9**, 874 (1991).
- [5] L. Kuipers, M. S. Hoogeman, and J. W. M. Frenken, *Phys. Rev. Lett.* **71**, 3517 (1993).
- [6] G. Danker, O. Pierre-Louis, K. Kassner, and C. Misbah, *Phys. Rev. Lett.* **93**, 185504 (2004).
- [7] H.-C. Jeong and E. D. Williams, *Surf. Sci. Rep.* **34**, 171 (1999).
- [8] F. Meyer zu Heringdorf, M. Reuter, and R. Tromp, *Nature (London)* **412**, 517 (2001).
- [9] K. Roos, K. Roos, M. Horn-von Hoegen, and F. Meyer zu Heringdorf, *J. Phys. Condens. Matter* **17**, S1407 (2005).
- [10] M. Hohage, M. Bott, M. Morgenstern, Z. Zhang, T. Michely, and G. Comsa, *Phys. Rev. Lett.* **76**, 2366 (1996).
- [11] R. Persaud, H. Noro, M. Azim, R. Milne, and J. Venables, *Scanning Microsc.* **8**, 803 (1994).
- [12] D. Reuter, G. Gerth, and J. Kirschner, *Phys. Rev. B* **57**, 2520 (1998).
- [13] H. Rotermund, *Surf. Sci.* **283**, 87 (1993).
- [14] R. Tromp and M. Reuter, *Ultramicroscopy* **36**, 99 (1991).
- [15] T. Michely, M. Reuter, and R. Tromp, *Phys. Rev. Lett.* **73**, 2095 (1994).
- [16] L. I. Chelaru and F.-J. Meyer zu Heringdorf, *Appl. Phys. Lett.* **89**, 241908 (2006).
- [17] H. Yeom, I. Matsuda, K. Tono, and T. Ohta, *Phys. Rev. B* **57**, 3949 (1998).
- [18] K. Jeong Kong, H. W. Yeom, D. Ahn, H. Yi, and B. D. Yu, *Phys. Rev. B* **67**, 235328 (2003).
- [19] M. Hanbücken, M. Futamoto, and J. Venables, *Surf. Sci.* **147**, 433 (1984).
- [20] E. Pehlke and J. Tersoff, *Phys. Rev. Lett.* **67**, 465 (1991).
- [21] T. R. Linderoth, J. J. Mortensen, K. W. Jacobsen, E. Lægsgaard, I. Stensgaard, and F. Besenbacher, *Phys. Rev. Lett.* **77**, 87 (1996).
- [22] P. A. Greaney and D. C. Chrzan, *Phys. Rev. B* **72**, 115432 (2005).
- [23] See EPAPS Document No. E-PRLTAO-99-053753 for a PEEM movie of the thermal decay of a Ag island on Si(001), produced *in situ* and in real time. For more information on EPAPS, see <http://www.aip.org/pubserv/epaps.html>.